# Inertial Confinement Fusion as a Tool to Study Fundamental Nuclear Science

Mark Yuly, Stephen Padalino, Tyler Kowalewski, Salvatore Ferri and Steven Raymond.

## Why use ICF to study fundamental nuclear science?

Inertial confinement fusion (ICF) may be used to make fundamental nuclear science measurements of low-energy light-ion cross sections that are of interest in astrophysics and fusion research. These reactions are very difficult to measure using standard accelerator techniques because the cross sections become very small at energies far below 1 MeV, and it would therefore take prohibitively long to collect satisfactory statistics. The thermonuclear reactions present in the inertial confinement fusion process, however, which occur during an interval of less than a nanosecond, result from raising a tremendously large number of nuclei to high temperatures at which the average energy of the nuclei is on the order of 10-20 keV. Thus, by using ICF, even reactions with very small cross sections can generate measurable numbers of product nuclei in a very short period of time. For example, using an accelerator producing a 1 μA triton beam at 25 keV it would take nearly 100 years of continuous beam to obtain one million $^{7}$Li(t,$\alpha$)$^{6}$He reactions. On the other hand, a single OMEGA shot doped with 1% of $^{7}$Li could produce the same number of reactions in less than 1 ns. Moreover, many of the most interesting reactions are tritium induced, and therefore not well-suited to accelerator study because of problems with tritium contamination.

## What could be measured?

Careful examination of the chart of nuclides reveals that most product isotopes that could be reached by zero-energy-threshold tritium radiative capture (t,$\gamma$), stripping (t,p) and (t,$\alpha$) reactions decay by beta emission with half-lives ranging from 20 ms to 10 s. Because the cross sections are so small, the number of prompt gamma rays or charged particles from these reactions is small compared to the number of primary neutrons, and therefore difficult to separate from the large prompt background pulse. However, by waiting until the prompt radiation has died away it may be possible to collect the product nuclei and count their radioactive decays in a much quieter radiation and electronic environment. This may allow cross sections to be measured with as few as several hundred product nuclei.

The 2018 report describes yield calculations for many light ion reactions that might be studied this way using the OMEGA laser at the Laboratory for Laser Energetics. These are summarized in Table 1, with the orange highlighted reactions being those with yields that may be measurable using OMEGA. The green highlighted reactions may become feasible with the 1000 times higher yields that may be possible at NIF. Comparison with cross section measurements at higher energies for reactions where measurements are available indicates these yield predictions may be as low by as much as a factor of 100.

**Table 1. Product half-life, reactant natural abundances, and predicted yields for a number of light ion reactions that may be studied using ICF.** The predicted yields are based on the yield of OMEGA shot 77951 which was a tritium-filled $SiO_2$ capsule "exploding pusher" having a 1 .5%-98.5% DT mixture and reaching an ion temperature of 18.3 keV. Reactivities were calculated using TALYS-1.9 [1] and the S-factor extrapolations of Abramovich et. al. [2]. No cross sections are available for $^{3}H(t,\gamma)^{6}He$ so the predicted yield is based on assuming a branching ratio of $10^{-7}$, which is simply an estimated "best case". For $^{11}B(d,p)^{12}B$ and $^{15}N(d,p)^{16}N$ for which data are available at higher energies, TALYS underpredicts the cross sections by as much as a factor of 100.

| Reaction | Product Half-life | Reactant Abund. | Predicted Yield |
|---|---|---|---|
| $^{3}H(t,\gamma)^{6}He$ | 807 ms | $^{3}H$ fill | $8\times10^{4}$ |
| $^{6}Li(t,p)^{8}Li$ | 840 ms | 7.6% | $4\text{-}16\times10^{5}$ |
| $^{7}Li(t,\alpha)^{6}He$ | 807 ms | 92.4% | $1\text{-}4\times10^{5}$ |
| $^{9}Be(t,\alpha)^{8}Li$ | 840 ms | 100% | $8\times10^{4}$ |
| $^{9}Be(t,\gamma)^{12}B$ | 20.2 ms | 100% | 3.0 |
| $^{10}B(t,p)^{12}B$ | 20.2 ms | 19.9% | 923 |
| $^{11}B(d,p)^{12}B$ | 20.2 ms | 80.1% | 1735 |
| $^{13}C(t,\gamma)^{16}N$ | 7.1 s | 1.1% | 0.1 |
| $^{13}C(t,\alpha)^{12}B$ | 20.2 ms | 1.1% | 108 |
| $^{13}C(t,p)^{15}C$ | 2.45 s | 1.1% | 17.7 |
| $^{14}N(t,p)^{16}N$ | 7.1 s | 99.6% | 2.5 |
| $^{15}N(d,p)^{16}N$ | 7.1 s | 0.4% | 2.0 |

## How would it work?

In order to measure these cross sections requires the development of a technique for trapping as many of these product nuclei as possible and counting their decays. After the shot, the ions from the reactions of interest slow down in the plasma, and eventually recombine and become thermalized. Three ways of collecting the now neutral reaction products are being considered:

1. **Turbomolecular or ion pump trap.** Gas atoms leaving the target enter a long tube placed as closely as possible to the target center. They travel to a turbopump or an ion pump where they are trapped. For the turbopump, the gas is trapped in the foreline where it is counted. For the ion pump, the atoms are re-ionized and accelerated into a titanium electrode where they implant and can be counted. Although most product nuclei do not enter the tube, assuming the

explosion is isotropic the known solid angle can be used to determine the fraction of the product collected. Even at room temperature these atoms will be moving fast enough to reach the trap in a few milliseconds.

2. **Getter.** Another possibility, for reactive products, would be to place a getter near the target. Product atoms would bind to the getter material where they could be counted.

3. **Evacuate the chamber.** In this case, a turbopump or cryopump would be used to completely evacuate the target chamber. This has the advantage of collecting all of the product nuclei with a known efficiency, but, unfortunately, experience with the Omega Gas Sampling System (OGSS) [3] leads to the expectation that it would require about 90 seconds, which is much longer than any of the product half-lives.

In order to study the feasibility of these various techniques, a test system, shown in Figure 1, has been built at Houghton College. The system was described in the previous report so only an overview will be given here. A 50.8 cm (20 in.) diameter, 15.24 cm (6 in.) high stainless-steel vacuum chamber is used to simulate the OMEGA target chamber. The chamber is evacuated by a water-cooled Pfeiffer TPH062 Turbomolecular pump backed by an Alcatel Pascal 2005 SD rotary forepump. Pressure is monitored using a Duniway T-075-N ionization gauge with a Varian Multigauge controller and a Granville-Phillips convectron gauge with a GP 275 controller. A Parker Precision Fluidics 009-0181-900 Ultra Low Leak Extreme Performance Valve allows extremely short bursts (as short as a few hundred microseconds) of gas into the chamber.

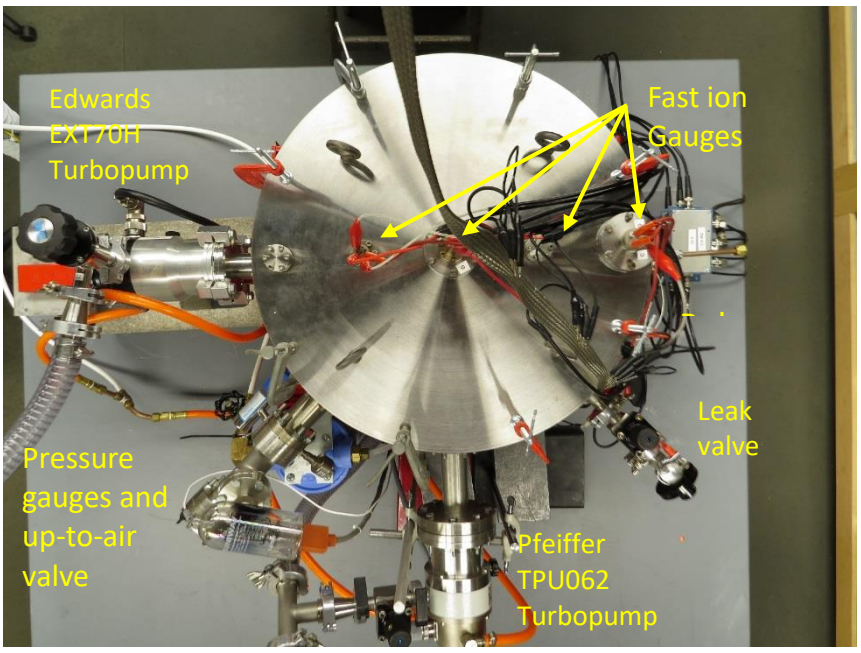


**Figure 1. The experimental test system.** Short bursts of gas are allowed to enter the chamber using the fast "pulse valve" and the motion of the pressure front can be tracked using the fast ion gauges. Different types of traps and detectors can be test using this apparatus. Current work is focused on using a turbomolecular drag pump as the trap.

## How can the gas collection and trapping techniques be tested?

In order to test this trapping technique, a radioactive gas with properties similar to the product nuclei in Table 1 is needed. Since the initial prototype trap using a turbopump is capable of pumping inert gasses like $^{6}$He which is the product of both $^{3}$H(t,$\gamma$)$^{6}$He and $^{7}$Li(t,$\alpha$)$^{6}$He, it was decided to find a similar test gas. The isotope $^{41}$Ar is such a nucleus. However, while it is an inert gas, it unfortunately beta decays with an endpoint energy of only 1.2 MeV compared to the 3.5 MeV endpoint energy of $^{6}$He. In fact, this endpoint is near the average energy for $^{6}$He of 1.57 MeV. This simply means any system that works with $^{41}$Ar would likely work even better, after recalibration, with the higher energy electrons from $^{6}$He. The 109 min half-life of $^{41}$Ar has the advantage of allowing it to be produced at SUNY Geneseo using the Pelletron or possibly even the PuBe source and brought to Houghton College to be inserted in to the test system, a 45 minute drive.

The $^{41}$Ar can be created via the reaction $^{40}$Ar(d,p)$^{41}$Ar, which has a cross section of about 0.2 b at 3 MeV. During the summer of 2018 a gas cell was constructed at SUNY Geneseo for the purpose of generating $^{41}$Ar for these experiments using their tandem Pelletron accelerator. It was found that the neutron radiation levels during this process were high which required extra safety precautions, and so an attempt is being made to use lower energy deuterons.

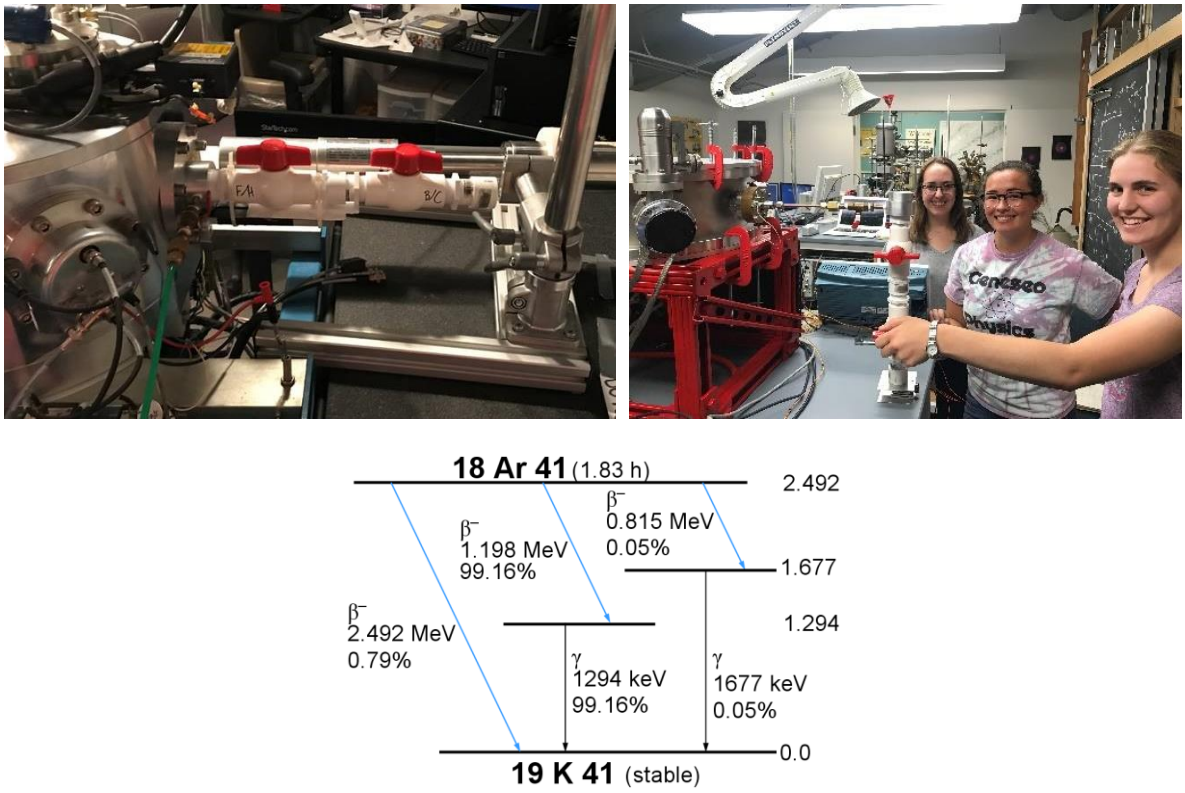


**Figure 2. The $^{40}$Ar gas cell and $^{41}$Ar decay scheme.** (Top left) The gas cell attached to the SUNY Geneseo 15R beam line scattering chamber. The cell was first filled with $^{40}$Ar, then irradiated with deuterons to produce $^{41}$Ar via $^{40}$Ar(d,p)$^{41}$Ar. (Top right) The gas cell containing $^{41}$Ar could then be transported to Houghton College and attached to the test chamber. (Bottom) The decay scheme for $^{41}$Ar, which beta decays with a half-life of 109 min to $^{41}$K [4].

The argon gas in the gas cell acts like a thick target. Deuterons entering the gas slow down and eventually stop, so although the $^{40}$Ar(d,p)$^{41}$Ar reaction can occur at any time the cross section for the reaction is decreasing as the deuterons penetrate deeper into the cell. In order to calculate the yield of $^{41}$Ar then, the cross section is needed for energies from the incident energy of the deuterons all the way down to zero. Since the only measurements to date [5] are between 3 and 7 MeV, it was necessary to estimate the cross sections for these low energies. The cross sections were calculated using TALYS-1.9 [1] and an attempt was made to fit the cross section using the R-Matrix code AZURE2 [6]. As can be seen in Figure 3, the two calculations agree roughly in magnitude with each other, but underpredict the measured cross section by about a factor of four at the higher energies.

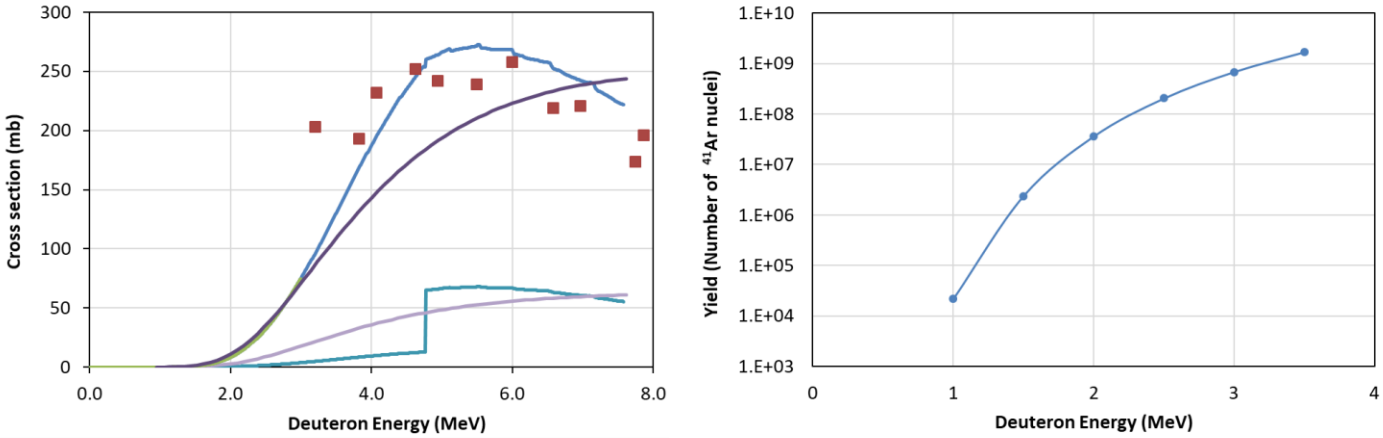


**Figure 3. Cross sections and expected yield for $^{40}$Ar(d,p)$^{41}$Ar.** (Left) Cross sections were measured [5] (red squares) and calculated using TALYS-1.9 [1] (light blue) and AZURE2 [6] (light purple). While the two calculations are roughly consistent with each other, they are approximately one-fourth the measured value at higher energies. Also shown are the AZURE result multiplied by 4 (dark purple) and the lower energy part of the TALYS result multiplied by 20 and the upper part by 4 (dark blue). The reason for the discontinuity is unclear. (Right) The predicted $^{41}$Ar yield for a 10 nA beam of deuterons striking a thick $^{40}$Ar target at STP for 1 half-life as a function of incident deuteron energy. These yields are based on the AZURE2 cross sections, and so may represent a low estimate.

The calculation of the $^{41}$Ar yield in the gas cell then has three distinct parts. First, the energy of the deuterons as a function of depth into the argon gas cell is needed. This can be found using

$$x(E') = \int_{E_0}^{E'} \frac{1}{\frac{dE}{dx}(E)} dE \qquad (1)$$

where $x(E')$ is the depth $x$ an incident deuteron of energy $E_0$ will penetrate before it has energy $E'$. The stopping power $\frac{dE}{dx}(E)$ is the rate at which the deuterons lose energy with distance and is a function of the deuteron energy $E$. A table of values for $dE/dx\,(E)$ in argon at STP was created using the code SRIM [7] and the integral was carried out numerically for various incident energies using cubic spline integration. These results created another table was then inverted to find $E(x)$ using cubic splines to

interpolate between values. This was also used to find the range of the deuterons, which for 2 MeV deuterons is about 5 cm.

Next, the number of deuterons remaining in the beam was determined as a function of depth, $N(x)$. Clearly, the number of deuterons that interact in a thickness $dx$ is proportional to the number of target nuclei $\rho\ dx$ and the number of incident deuterons $N(x)$ where $\rho$ is the number density of argon nuclei in the gas. Therefore, the change in the number of deuterons in the beam $dN$ is

$$dN = -\sigma_{TOT}(E(x))\ \rho\ N(x)\ dx \tag{2}$$

where the total cross section $\sigma_{TOT}$ is a function of the deuteron energy. Integrating this expression yields

$$N(x) = N_0 e^{-\rho \int_0^x \sigma_{TOT}(E(x))dx}. \tag{3}$$

Since the $(d,p)$ reaction is the largest cross section reaction with argon that would remove the deuterons from the beam, the $^{40}$Ar(d,p)$^{41}$Ar cross section $\sigma(E)$ was used to approximate $\sigma_{TOT}(E)$. Using the extrapolated AZURE2 cross section $\sigma(E)$ described above shows that nuclear reactions remove very few deuterons from the beam before the deuterons stop.

Finally, the number of $^{41}$Ar produced can be determined. The rate $dN_{Ar}/dt$ at which $^{41}$Ar nuclei are produced in thickness $dx$ at a given depth $x$ into the argon is given by

$$\frac{dN_{Ar}}{dt} = \sigma\big(E(x)\big)\ N(x)\ \rho\ dx - \lambda N_{Ar} \tag{4}$$

where the first term is the rate of creation and the second term the rate at which the $^{41}$Ar nuclei decay with decay constant $\lambda$. Integrating over time yields the number created in each slice of thickness $dx$ a depth $x$ into the argon.

$$dN_{Ar}(x) = \frac{\rho\ N(x)\ \sigma(E(x))}{\lambda}\ \left(1 - e^{-\lambda t}\right) dx \tag{5}$$

where $t$ is the irradiation time. Finally, integrating over all the slices gives the total number of $^{41}$Ar nuclei

$$N_{Ar} = \frac{\rho}{\lambda}\left(1 - e^{-\lambda t}\right) \int_0^L N(x)\ \sigma(E(x))\ dx. \tag{6}$$

The results of this calculation for a 10 nA beam of deuterons stopping in a thick argon target at STP are shown in Figure 3 as a function of deuteron energy. These were computed using the AZURE2 cross section predictions. Even for energies less than the 2.2 MeV deuteron binding energy there is a significant yield, so it should be possible to carry out our future $^{41}$Ar experiments at lower energy in order to reduce the amount of neutron production and the associated radiological hazard.

## Can $^{41}$Ar be produced, trapped, and detected with the test system?

The initial experiment using the test system took place after the 2018 report was submitted, and so the results will be reported here. The purpose of this test was to see whether $^{41}$Ar could be produced, transported to Houghton College, injected into the test system, trapped, and detected.

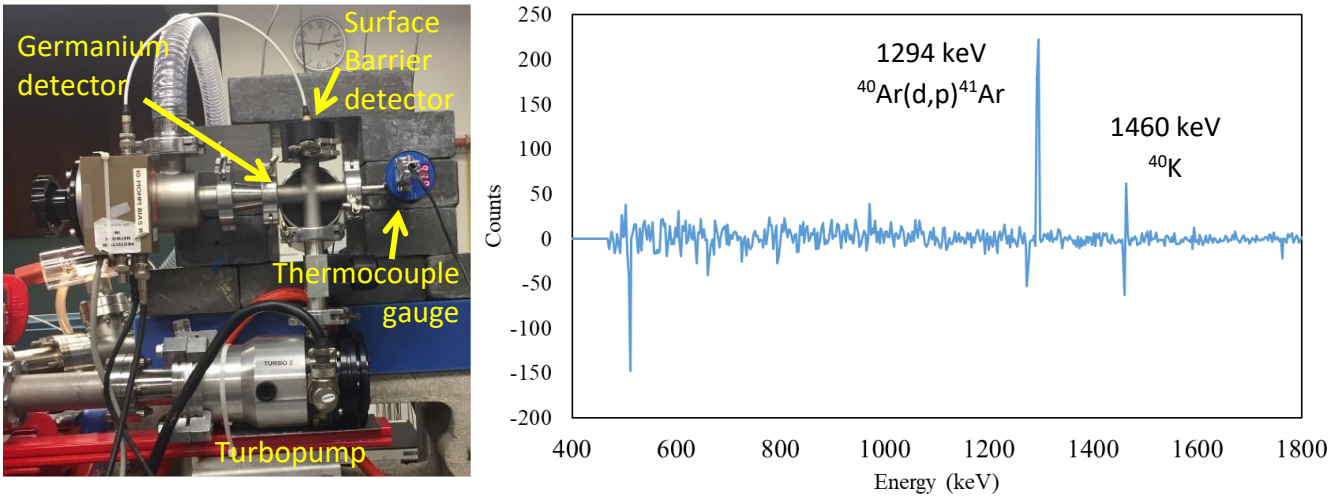


**Figure 4. Foreline counting system and gamma spectrum.** (Left) The gas traveed down the tube and was trapped by the turbopump in a "cross" attached to the foreline port. The cross could be isolated from the forepump by a valve. The pressure in the cross was monitored with a thermocouple gauge, the beta decays were counted with a silicon surface barrier detector, and the gamma rays with a germanium detector. (Right) The background subtracted gamma ray spectrum obtained in the experiment.

The tandem Pelletron at SUNY Geneseo produced a 30 nA beam of 3 MeV deuterons, which traveled across the 15R beam line scattering chamber and crossed from the vacuum into the argon-filled gas cell through a thin Kapton window. The argon gas in the gas cell was irradiated for one hour, then the gas cell was removed from the beamline and placed into a lead-shielded counting station where a 3-inch diameter HPGe detector counted gamma rays for approximately 4.5 hours. The gamma ray spectrum obtained exhibited a strong 1274 keV peak due to beta decay and subsequent de-excitation of the first excited state of $^{41}$K, as well as a much smaller 1677 keV peak resulting from beta decays to the second excited state. Other peaks in the spectrum were due to activation of chlorine in the PVC of the gas cell by $^{35}$Cl(d,p)$^{36}$Cl and possibly $^{35}$Cl(d,$\gamma$)$^{37}$Ar. Natural $^{40}$K decay was also visible.

After this test, the gas cell was returned to the 15R beamline, refilled with argon gas, and irradiated with 3 MeV deuterons for 2 hours. The next 45 minutes were spent transporting the gas cell to Houghton College, during which time a survey meter was used to monitor the cell to ensure no gas was escaping. The gas cell was then attached to the test system, and a rotary fore pump used to evacuate the transfer lines. The argon was then released into the transfer line, and the fast valve used to release a 1 ms pulse of gas into the test system vacuum chamber. For this test, the trap was the Edwards EXT70H turbomolecular drag pump attached to a long stainless-steel tube of approximately 4 mm inside diameter that extended directly across the chamber to 2 cm directly in from of the orifice of the fast valve. A four-way "cross" was attached to the turbopump foreline, in which the gas would be trapped

and decays counted by the HPGe detector located beside the cross and an ORTEC LEC 500-3000 silicon beta detector located at one end, as shown in Figure 4.

Figure 4 also shows the gamma ray spectrum obtained by counting the gas trapped in the foreline cross for 109 min, one half-life of $^{41}$Ar. The events in the 1294 keV peak were selected and binned into 1 min time bins, and integrated over time. The resulting growth curves were fit with the function

$$N(t) = A\left(1 - e^{-\lambda t}\right) + Bt + C \qquad (7)$$

where A, B, and C and $\lambda$ are fit parameters. The parameter $\lambda$ is the decay constant for $^{41}$Ar, the parameter A is the total number of $^{41}$Ar decays, B is the constant background rate, and C is the number of total number of counts recorded before and after the gas enters the cross. A similar binning, integrating and fitting procedure was followed for the silicon detector. The results of fitting, shown in Figure 5, gave a half-life of $109.9 \pm 6.6$ min and $2590 \pm 239$ total beta decay events for the silicon detector and $119.1 \pm 12.2$ min and $1042 \pm 81$ events for the HPGe detector.

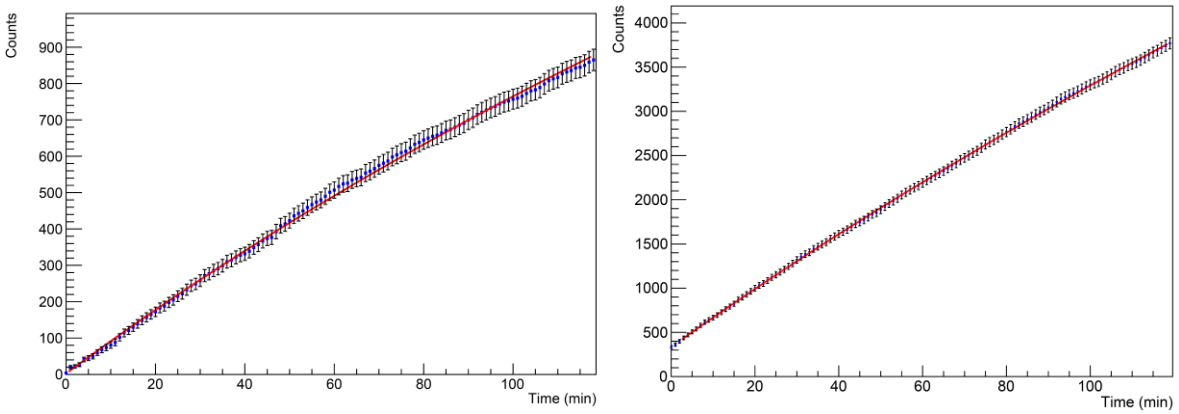


**Figure 5. Growth curves.** Integrated number of counts for the HPGe detector (left) and silicon detector (right), in one-minute time bins. The fit of Equation (7) is also shown (red line).

## Can the absolute efficiency of the detector be made adequate?

It is clear from the previous experiment that we were able to make, release, trap and collect $^{41}$Ar nuclei, but the fraction of decay events detected compared to the number of $^{41}$Ar nuclei created was very small, on the order of $10^{-6}$. The time required to bring the gas cell to Houghton College and attach it to the system only accounted for about a factor of two. Gas could have leaked out during transport, and certainly not all of the gas was released by the valve or collected by the tube. Another obvious reason for the low number of detected events is the very small solid angle for each of the two detectors. Needless to say, in order to be able to detect the very small number of beta decay events from product nuclei after an ICF implosion, we need to improve this number. One obvious starting point is to develop a detector with a much larger absolute efficiency.

A hollow box phoswich detector has been constructed that should have nearly 100% absolute efficiency for detecting beta particles released by gas trapped within its inner volume. Figure 6 shows the construction of the detector, which has an inner volume of 406.2 cm$^{3.}$ One end of the detector has a ½

inch-NPT threaded hole to accept a QF-16 flange for attaching the detector to the foreline of the turbopump. The opposite end of the detector is optically coupled with Eljen Technologies EJ-550 optical grade silicone grease to an ADIT B133D01 130 mm (5 inch) photomultiplier tube. This works but is less than satisfactory because the face of the PMT is not perfectly flat – it bows inward – meaning that more grease was needed in the center resulting in less transmission there. Another tube, a 130 mm (5-inch) ET Enterprises 9823KB with supposedly superior gain and timing characteristics, was intended for use, but as of this date is not working.

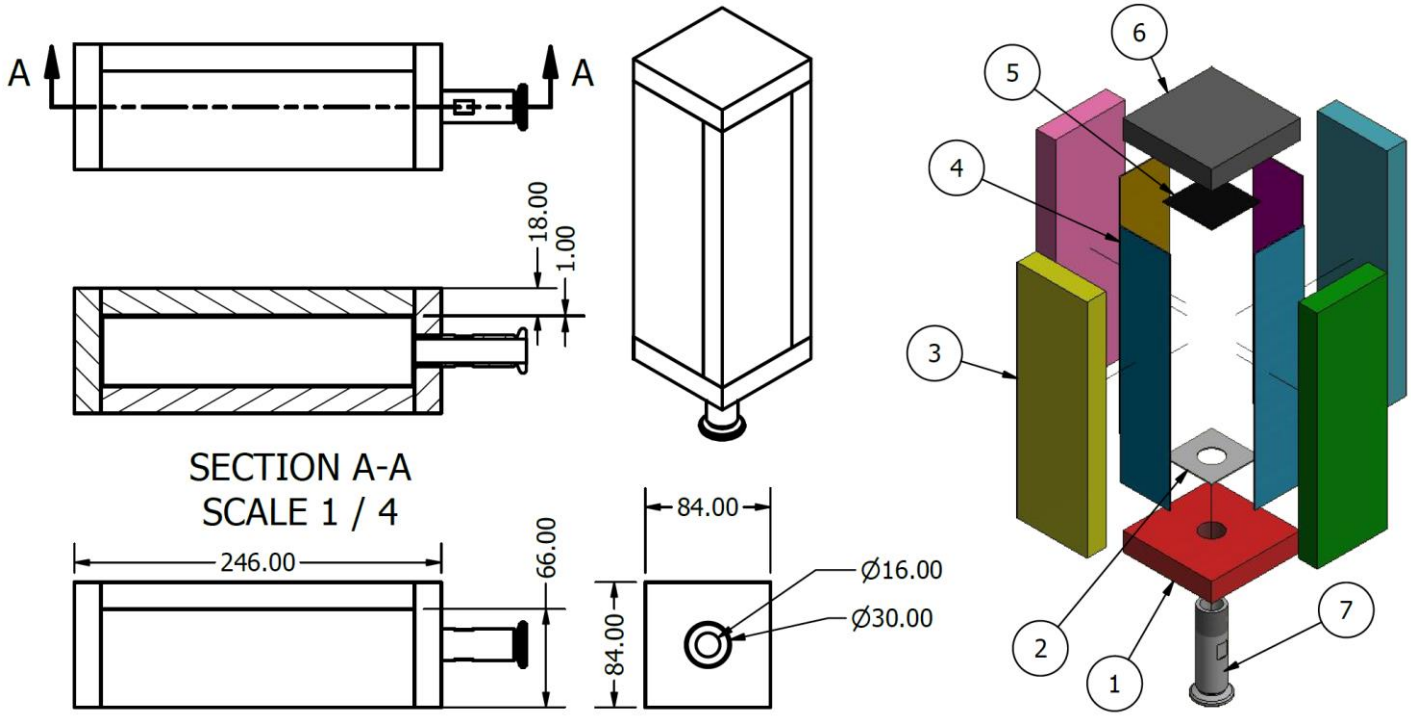


**Figure 6. Hollow phoswich detector.** The phoswich detector is a rectangular prism made of plastic scintillator, an outer thick layer made using slow scintillator material, and a thin inner lining made with fast scintillator. All dimensions are in mm.

The detector is called a phoswich detector because it is a "phosphor sandwich", that is, it uses two different phosphors, one fast and one slow, sandwiched together in a way that allows it to be read out by a single phototube. The box consists of an outer 18 mm thick shell of Eljen Technology EJ-240 plastic scintillator which has a decay time of 285 ns with a thin inner lining of 1 mm thick Eljen Technology EJ-212 plastic scintillator with decay constant of 2.4 ns. To assemble it, first the pieces were rough cut, then the edges were milled, and finally the milled edges that were not to be epoxied were polished. To polish, the milled edges were first sanded with 600 grit paper, washed with soapy water, then with 1500 grit paper and washed again. Then the edges were polished with Novus 7100 plastic polish, washing the pieces between each step. At the end of the process, the parts were washed with isopropanol. Each step was carried out in a different location to reduce the change of grit from a previous step causing scratches.

In the first attempt at assembling the detector, Eljen Technology EJ-500 optical cement was used. Prior to applying epoxy, all mating surfaces were roughened with 400 grit sandpaper then washed with isopropanol. Next, pairs of the thick side pieces were epoxied creating two L-shaped pieces. The thin inner lining pieces were epoxied into each L shape, then the L-shapes were epoxied together to form a hollow square tube. The inside of the tube was polished using the technique above. At this point, it was realized that the EJ-500 optical cement was not forming very strong bonds and in fact had separated in a few places. Also, since it was very thin, about the viscosity of water, it would not fill gaps. Unfortunately, in the gluing process the ends of the pieces were not perfectly lined up so there were about 0.5 mm ridges where they touched that could not be filled with epoxy. At this point, experiments were carried out with Pacer PT35 Zap Z-Poxy 15 Minute Epoxy, PC Products PC-Clear Two-Part Epoxy, Devcon 2 Ton Epoxy and Bob Smith Industries BSI-201 Quik-Cure Epoxy. The Devcon 2 Ton Epoxy was selected for its longer set time, its viscosity and its good transparency. The Devcon epoxy was then used to finish the first detector, and a second detector was also constructed according to the procedure above, but using the Devcon epoxy for all joints except for adhering the thin to the thick plastic. The Devcon epoxy was smeared on the threads of the NPT to QF-16 flange which was then screwed into the detector. The second detector was then successfully vacuum tested.

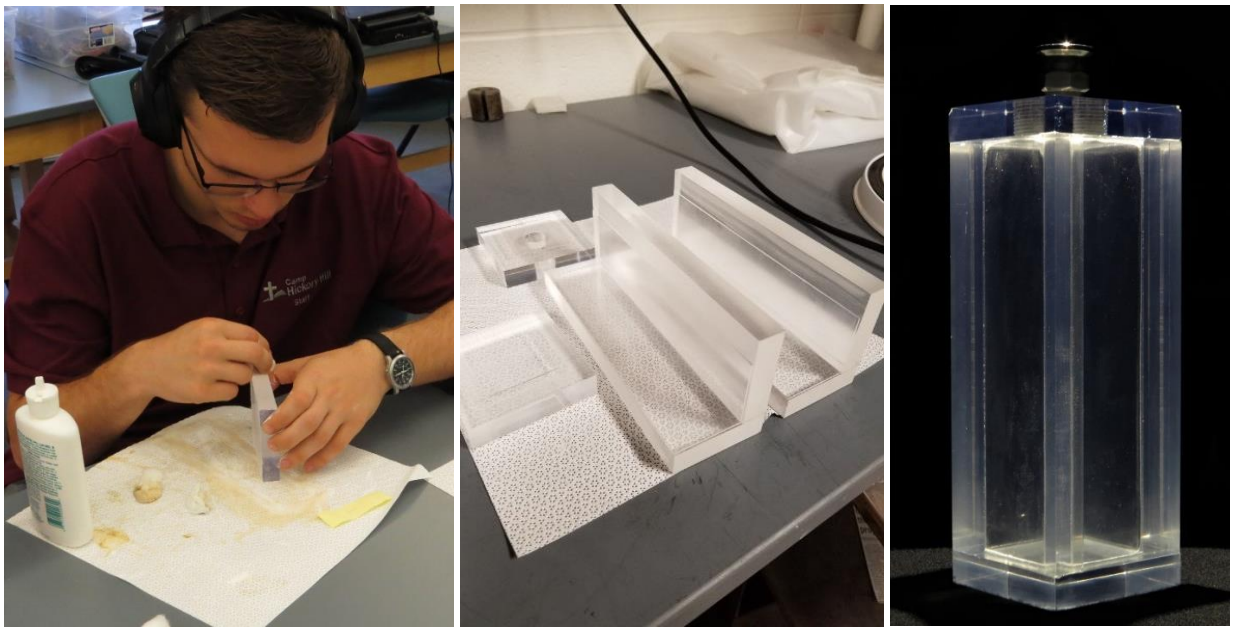

**Figure 7.** (Left) Houghton Student Tyler Kowalewski polishing the edges of the scintillator. (Center) The cut and polished pieces, with the two L-shapes already epoxied. (Right) The finished detector.

In order to use this detector for particle identification, the fast and slow components of the light pulse must be separated electronically. This means that preserving the shape of the PMT output pulse is very important, and so the output of the PMT base needs to be coupled directly to the anode. This required special negative high-voltage resistor divider bases to be constructed, as shown in Figure 8.

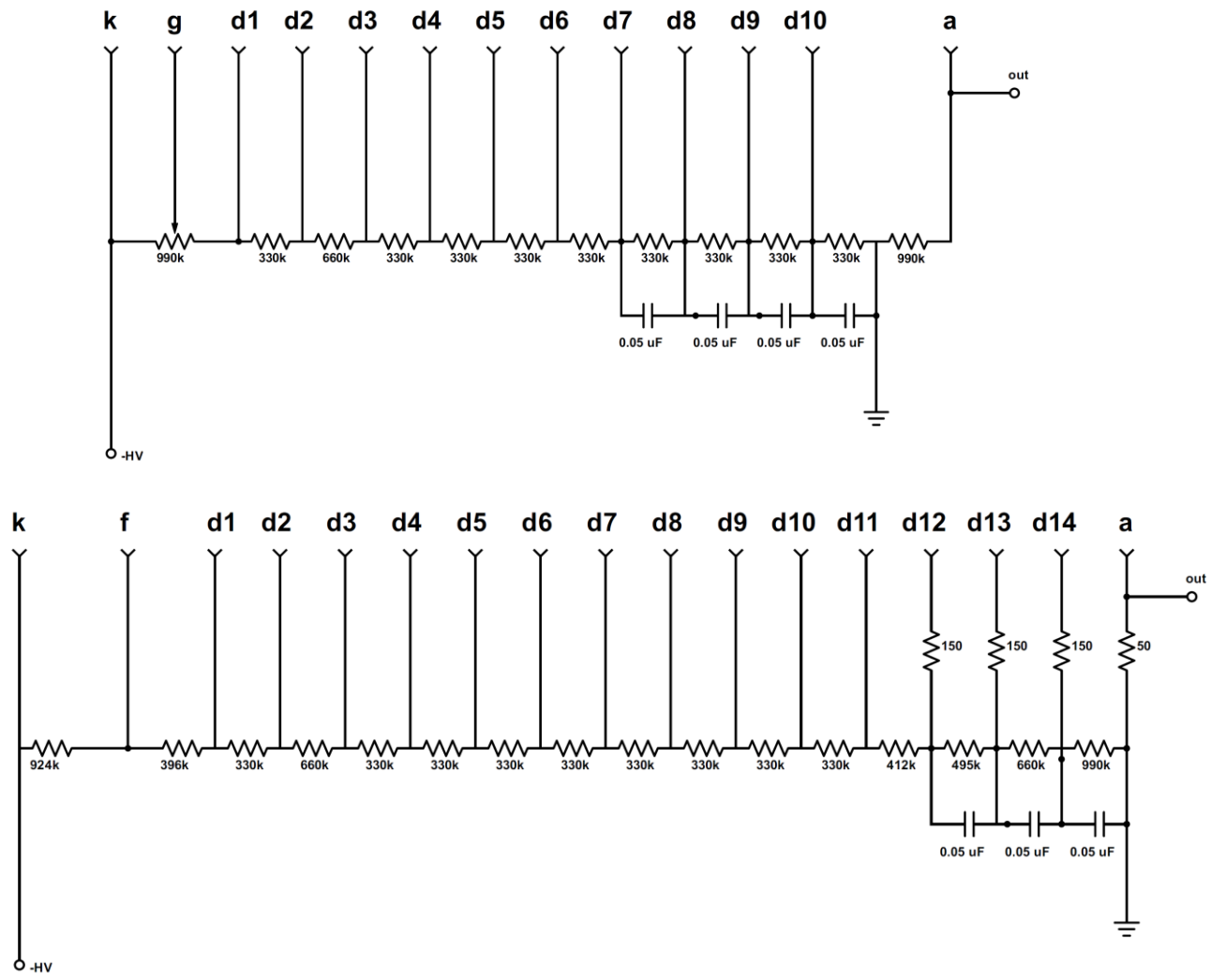


**Figure 8. Photomultiplier voltage dividers.** These schematics show the negative high-voltage dividers used in the bases for the ADIT B133D01 (top) and ET Enterprises 9823KB (bottom) phototubes.

The circuit shown in Figure 9 was constructed using NIM modules to separate the fast and slow components of the PMT signal so that they could be separately digitized by the FemtoDAQ data acquisition system. The FemtoDAQ accepts signals between -1 and 1 volts, so much of the difficulty in designing the circuit resulted from trying to match this. In order for the signals from the B133D01 PMT, which is a relatively low gain tube, to be large enough to trigger the CFD on small pulses, it was necessary to first amplify the PMT signal by 10 times. However, this resulted in pulses that were too big for the FemtoDAQ inputs after their values were sampled and held by the linear gates. For this reason the pulses were attenuated before entering the linear gates.

The constant fraction discriminator triggered on pulses larger than a certain minimum. This logic pulse was used three ways. First, it formed the gates for two linear gates: one that enclosed the fast component of the pulse, and one for the slow component. The linear gates produced an output that was proportional to the largest input voltage that came when the gate signal was present. The outputs

of the two linear gates were digitized by the FemtoDAQ. The third output from the constant fraction discriminator was used to form the external trigger for the FemtoDAQ that lets it know when to digitize. The circuit converted the fast negative NIM pulses first to TTL levels, then to the 3.3V CMOS levels needed by the FemtoDAQ.

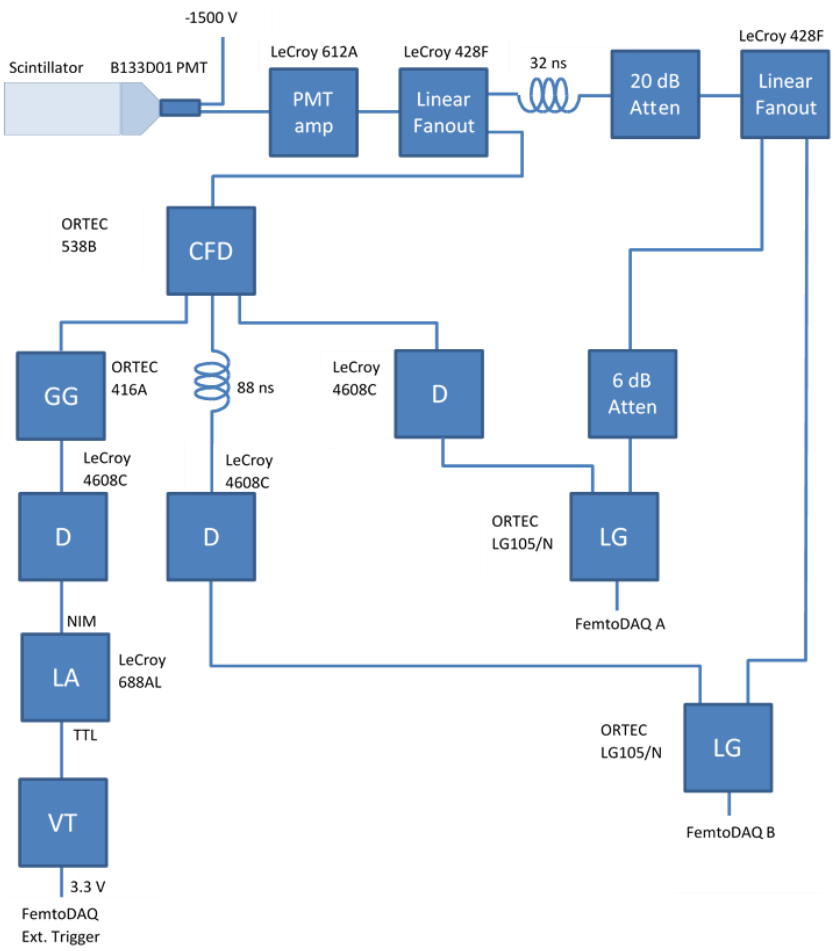


**Figure 9. Schematic diagram of the phoswich detector system**. This circuit separated the slow and fast components of the PMT pulses. In this diagram, CFD stands for constant fraction discriminator, D for discriminator, GG for gate generator, LG for linear gate, LA for level adapter and VT for voltage translator.

Typical signals at various places in the circuit of Figure 9 are shown in Figure 10. Because the B133D01 tube is relatively slow, 25 ns FWHM for a fast scintillator pulse, the gates were set to switch between fast and slow at about 50 ns past the maximum of the peak. The FPGA code in the FemtoDAQ has a bug that causes the internal digitizer to begin about 400 ns before the external trigger is received; this is the reason the external trigger pulse was coming so late into the output pulses from the linear gates, which were very long pulses, almost 3 μs long.

Figure 11 shows typical 2D histograms produced by putting different sources into the detector. The $^{207}$Bi source is unusual because it produces monoenergetic electrons of energy 480 keV and 967 keV. The

electrons near 1 MeV were easily separated from the other events by the detector. The background histogram mostly contains events that only deposited energy in the thick scintillator. For gamma rays this is because the thick scintillator was so much thicker so the gamma rays were much more likely to interact, and for charged particles it is because they were coming from outside so they always had a large pulse in the outer scintillator. This reverses for the case of placing an alpha source inside the detector. In this case, the alpha particles could not penetrate the thin inner scintillator, so all the energy was deposited in the thin inner scintillator.

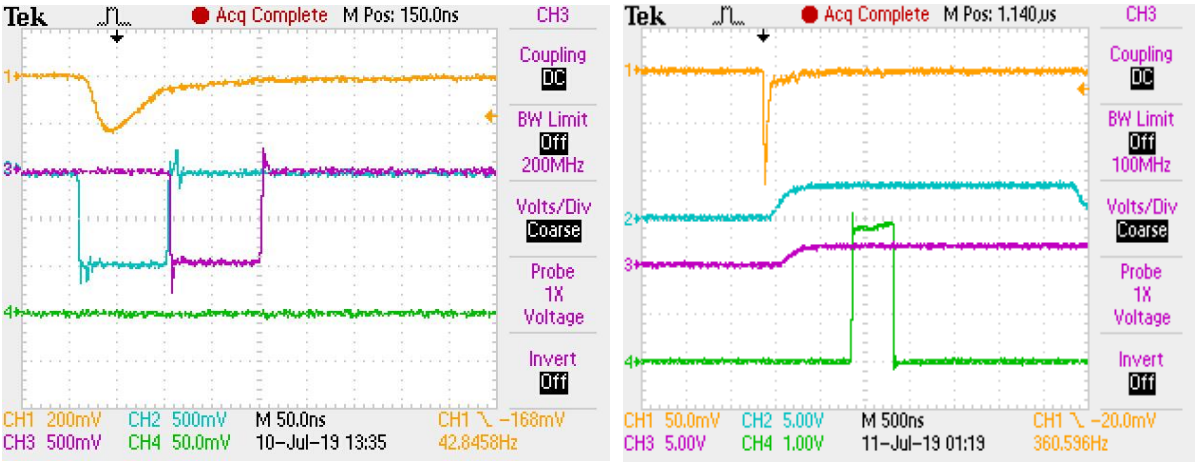


**Figure 10. Typical analog PMT pulses and logic pulses for the $^{207}$Bi source.** The signal from the PMT (orange) was used to create the gates for the fast (blue, left) and slow (purple, left) components of the light pulse from the scintillator. The linear gates produced an output that was proportional to the maximum input voltage when the gate signal was active, for the fast component gate (blue, right) and slow component (purple, right). The external trigger (green, right) told the FemtoDAQ when to digitize the voltage.

## Can the detector efficiency be measured?

An experiment is being carried out to measure the efficiency of the new phoswich detector using $^{41}$Ar produced using the accelerator at SUNY Geneseo. For this test, the gas cell will be attached to the end of the 15R beamline on the SUNY Geneseo Pelletron, filled with argon, and irradiated for 2 hours with a 10 nA beam of 2 MeV deuterons. The gas cell will then be brought to the counting station, shown in Figure 12, where it will be attached to the transfer line so that the argon in the cell can enter the phoswich detector. The air will be removed from the transfer line and phoswich detector by a rotary pump, then the valves will be opened allowing the gas to enter the detector where it will be counted for several hours.

Also attached to the apparatus, just above the phoswich detector, is an ORTEC LEC 500-3000 silicon beta detector that will be used to provide the efficiency calibration. The silicon detector is very nearly 100% efficient for detecting electrons that strike it and deposit energy above the lower level set by the trigger discriminator. This means that the true number of $^{41}$Ar decays per unit volume in the argon gas can be determined from the number detected by the silicon detector simply by scaling by a geometrical factor, which can be calculated, that accounts for the fraction of decays occurring in the region visible to the

silicon detector that produce electrons that enter the detector. Once the number of $^{41}$Ar per unit volume is known, it can be used to determine the absolute efficiency of the phoswich detector.

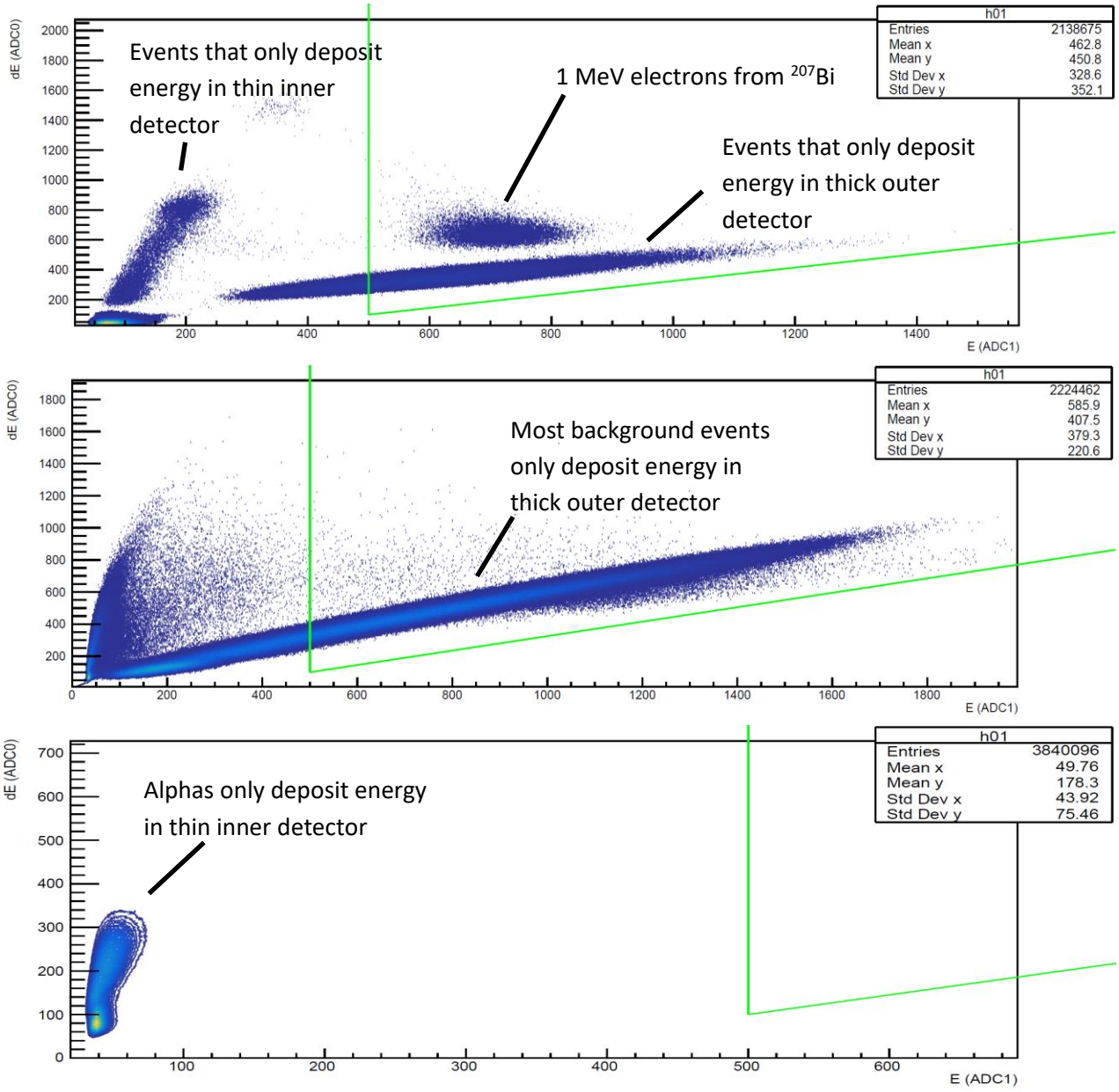


**Figure 11. 2D dE-E Histograms**. The pulse height from the thin inner dE scintillator (fast component) is plotted versus the thick slow E scintillator (slow component) for a $^{207}$Bi electron source inside the detector (top), background radiation (middle) and a $^{241}$Am alpha source inside the detector (bottom).

The one obvious problem with this scheme for calibrating the efficiency is that it does not take into account the events that are missed because they produce pulses smaller than the cutoff threshold of the discriminator. This would not be a problem if both the phoswich and silicon detectors had the same threshold, but this is unlikely. However, by using the $^{207}$Bi monoenergetic electron source it should be possible to calibrate the energy scale so that the thresholds of the two detectors are known, and a

correction can be made using the known shape of the beta decay spectrum. One possible way to do this would be to use the code GEANT 4 simulate the setup.

**Figure 12. Experiment setup.** (Left) Houghton students (left to right) Salvatore Ferri, Steven Raymond, and Tyler Kowalewski assembling the detector system at SUNY Geneseo. (Right) The $^{41}$Ar is prepared in the white PVC gas cell at the right of the photograph. Air is removed from the transfer line and the detector by the rotary pump, then the valve will allow the argon to enter the black detector on the left side which will count $^{41}$Ar decays.

## What about background rates at OMEGA?

One of the primary advantages of the technique being developed in this project is that it allows the decays of the product nuclei to be detected long after the laser shot, in the quiet radiation environment after the prompt radiation has passed. The purpose of the OMEGA ride-along experiment currently planned for October 9, 2019 is to test this assumption, as well as the ability of the detector and electronics to survive the EMP, and to turn on quickly and begin counting within a few milliseconds after the shot.

For this experiment, the phoswich detector will be placed near the OMEGA target chamber, connected to a RG-58 signal cable and an RG-59 cable for high voltage. The cables will run from the detector to the NIM electronics which will be in LaCave. Figure 13 shows a block diagram of the planned experiment. A signal from the OMEGA control room indicating the timing of the laser shot will cause the control Arduino to wait for about a millisecond, then, as shown in Figure 14, turn on four MOSFET switches to activate four 15 kV high-voltage isolation reed relays that will switch on the high voltage to the detector and connect the signal to the electronics. The control Arduino will also signal to the FemtoDAQ to begin to prepare for collecting data, causing the FemtoDAQ to start its FPGA with the necessary parameters. After waiting an appropriate amount of time, the Arduino will then release the veto signal allowing the FemtoDAQ to begin collecting events. The FemtoDAQ FPGA is capable of collecting events with zero dead time for intervals as long as 45 seconds before it has to read out. Many of these intervals will be strung together to collect background data spanning the time scales from milliseconds to minutes after the shot.

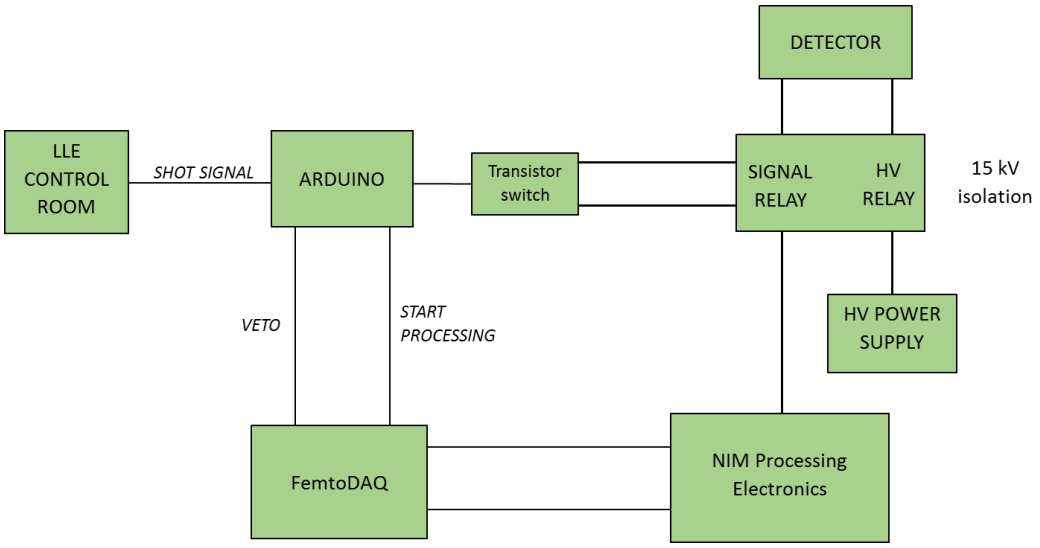


**Figure 13. Electronics setup for the ride-along experiment at LLE.** Prior to and during the laser shot, the electronics will be electrically isolated from the detector. A signal indicating the timing of the laser shot will start the Arduino controller, which will wait for about 1 ms before turning on the transistor switches which the close the HV isolation reed relays. About 2 ms later, the Arduino will signal the FemtoDAQ to begin collecting data.

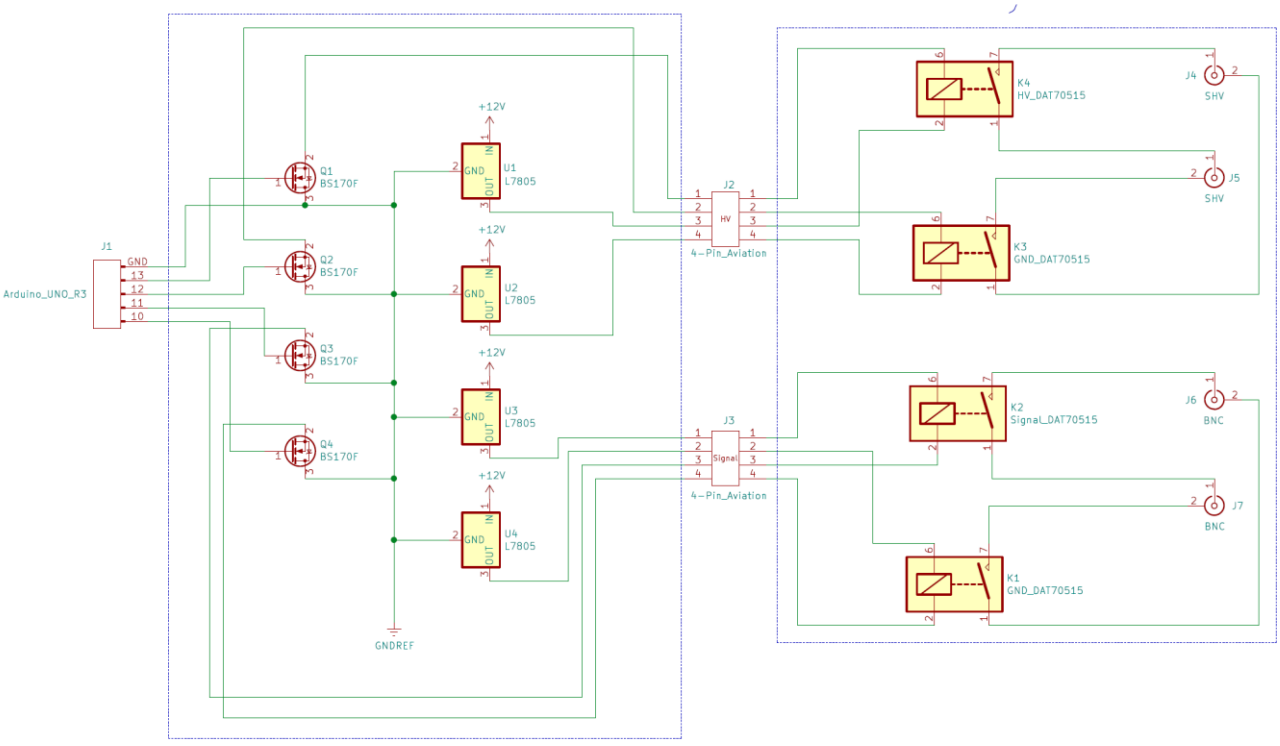


**Figure 14. Circuit diagram for the relay isolation controller.** Four Arduino output ports are used to switch four MOSFETs which in turn close four 15 kV isolation reed relays. These relays switch individually the signal, signal ground, high voltage and high voltage ground.

## What are the long-term plans?

Earlier this year we submitted a letter of intent to submit a proposal for the Nuclear Data Interagency Working Group / Research Program (DE-FOA-0002114) to fund this research. The plan was to spend one year evaluating different techniques for trapping and detecting the decaying product nuclei, one year on an engineering study and constructing a laboratory diagnostic grade detector, and one year collecting cross section data. Based on the letter of intent we were invited to submit a full proposal, but upon further consideration we decided that it would be better to wait and attempt to write the proposal next year, when we had more time to prepare the document and after spending one more summer doing preliminary measurements.

In the future, experiments must be done using the test chamber to release radioactive gasses, such as $^{41}$Ar, to test how well they can be captured using the three techniques that we consider most likely to work – using a turbopump trap, an ion pump trap, and, for chemically reactive substances, the getter trap. Hopefully by the end of this summer the work on detectors and preparing $^{41}$Ar will have progressed to the point that these experiments will become possible.

## Presentations and awards since summer 2018

**Award**

Katelyn Cook, 2019 Apker Award Finalist, *"For her experimental contributions toward the measurement of low-energy nuclear cross sections using inertial confinement fusion."*

**Poster**

Katelyn Cook, Emma Bruce, Sarah Hull, Mark Yuly, Stephen Padalino, Craig Sangster, and Sean Regan. "Measuring Low Energy Nuclear Cross Sections using ICF," Omega Laser User's Group Meeting, Laboratory for Laser Energetics, Rochester, NY, April 24, 2019; XXXVIII Annual Rochester Symposium for Physics Students, University of Rochester, March 30, 2019; 60th Annual Meeting of the APS Division of Plasma Physics, Portland, Oregon, November 5-9, 2018; Fifth Joint Meeting of the Nuclear Physics Divisions of the APS and JPS, Waikoloa Village, Hawaii, Oct. 23-27, 2018.

**Talk**

Cook, K. and Yuly, M. (March 30, 2019, 2018). "Measuring Low Energy Nuclear Cross Sections using Inertial Confinement Fusion." XXXVIII Annual Rochester Symposium for Physics Students, University of Rochester (Rochester, NY).

*This material is based upon work supported by the Department of Energy [National Nuclear Security Administration] University of Rochester "National Inertial Confinement Program" under Award Number(s) DE-NA0004144.*



[1] A.J. Koning, S. Hilaire and M.C. Duijvestijn, "TALYS-1.0", Proceedings of the International Conference on Nuclear Data for Science and Technology, April 22-27, 2007, Nice, France, editors. O.Bersillon, F.Gunsing, E.Bauge, R.Jacqmin, and S.Leray, EDP Sciences, 2008, p. 211-214.
[2] S.N. Abramovich, B.Ya. Guzhovskij, V.A. Zherebtsov, and A.G. Zvenigorodskij, International Nuclear Data Committee Report INDC(CCP)-326/L+F, (1991).
[3] M. A. Stoyer, C. A. Velsko, B. K. Spears, D. G. Hicks, G. B. Hudson, T. C. Sangster, and C. G. Freeman, Rev. Sci. Instrum. **83**, 023505 (2012).
[4] Nucleonica Wiki, https://www.nucleonica.com/wiki/index.php?title=Decay_Schemes#18_Ar_41_.28Z.3D18.2C_N.3D23.29.
[5] J.W.Engle,G.W.Severin,T.E.Barnhart,L.D.Knutson, and R.J.Nickles, Applied Radiation and Isotopes **70**, 355 (2012).
[6] R. E. Azuma, E. Uberseder, E. C. Simpson, C. R. Brune, H. Costantini, R. J. de Boer, J. Gorres, M. Heil, P. J. LeBlanc, C. Ugalde, and M. Wiescher. Phys. Rev. C **81**, 045805 (2010).
[7] J.F. Ziegler, J.P. Biersack, and M.D. Ziegler, *SRIM – The Stopping and Range of Ions in Matter,* (Ion Implantation Press, 2008).